Research Square

Preprints are preliminary reports that have not undergone peer review.
They should not be considered conclusive, used to inform clinical practice,
or referenced by the media as validated information.

Longitudinal multimodal evaluation of craniofacial growth during complete denture rehabilitation in a child with X-linked hypohidrotic ectodermal dysplasia: a 7-year observational study

Jin Guo
Department of Prosthodontics, School and Hospital of Stomatology, Hebei Medical University
Zhe Sun
Department of Prosthodontics, School and Hospital of Stomatology, Hebei Medical University
Xiaoping Ma
Dental Laboratory, School and Hospital of Stomatology, Hebei Medical University
Yunlu Zhao
Hebei University of Chinese Medicine, Institute of Integrated Chinese and Western Medicine
Xia Qi
Department of periodontics , School and Hospital of Stomatology, Hebei Medical University
Dong Han
Department of Prosthodontics, Peking University School and Hospital of Stomatology
Yunyun Yuan
Department of Prosthodontics, School and Hospital of Stomatology, Hebei Medical University
Ya Zhao
Department of Prosthodontics, School and Hospital of Stomatology, Hebei Medical University
Jiabao Ren
Department of Prosthodontics, School and Hospital of Stomatology, Hebei Medical University
Wenjing Shen
wenjingshen2020@hebmu.edu.cn

Hebei Medical University

Research Article

Keywords: X-linked hypohidrotic ectodermal dysplasia, congenital anodontia, craniofacial development, complete denture rehabilitation, cone-beam computed tomography, three-dimensional imaging, longitudinal study

Posted Date: November 12th, 2026

DOI: https://doi.org/10.21203/rs.3.rs-11090570/v1

License: This work is licensed under a Creative Commons Attribution 4.0 International License.
Read Full License

Additional Declarations: No competing interests reported.

Longitudinal multimodal evaluation of craniofacial growth during complete denture rehabilitation in a child with X-linked hypohidrotic ectodermal dysplasia: a 7-year observational study

Jin Guo[1], Zhe Sun[1], Xiaoping Ma[2], Yunlu Zhao[3], Xia Qi[4], Dong Han[5], Yunyun Yuan[1], Ya Zhao[1], Jiabao Ren[1*], Wenjing Shen[6*]

1. Department of Prosthodontics, School and Hospital of Stomatology, Hebei Medical University & Hebei Key Laboratory of Stomatology, Shijiazhuang 050017, China

2. Dental Laboratory, School and Hospital of Stomatology, Hebei Medical University, Shijiazhuang 050017, China

3. Hebei University of Chinese Medicine, Institute of Integrated Chinese and Western Medicine, Shijiazhuang 050017, China

4. Department of periodontics Ⅰ, School and Hospital of Stomatology, Hebei Medical University & Hebei Key Laboratory of Stomatology, Hebei Technology Innovation Center of Oral Health, Shijiazhuang, China

5. Department of Prosthodontics, Peking University School and Hospital of Stomatology & National Center for Stomatology & National Clinical Research Center for Oral Diseases & National Engineering Research Center of Oral Biomaterials and Digital Medical Devices & Central Laboratory, Beijing 100081, China

6. Hebei Medical University & Hebei Key Laboratory of Stomatology, School and Hospital of Stomatology, Shijiazhuang 050017, China

[*]Correspondence:

Jiabao Ren, Email: renjiabao2012@163.com

Wenjing Shen, Email: wenjingshen2020@hebmu.edu.cn

Abstract

Background

X-linked hypohidrotic ectodermal dysplasia is frequently associated with severe tooth agenesis and craniofacial abnormalities. Long-term quantitative evidence integrating skeletal and prosthetic changes during childhood remains limited. This study characterized changes over 7 years of complete-denture rehabilitation and quantified the immediate facial soft-tissue response to denture insertion in a child with genetically confirmed X-linked hypohidrotic ectodermal dysplasia and congenital anodontia.

Methods

This retrospective longitudinal case study followed a male child from 7 to 14 years of age. Craniofacial changes were assessed using cephalometry and anterior cranial-base voxel-based superimposition of cone-beam computed tomography images. Prosthetic changes were evaluated through digital three-dimensional analysis of complete dentures obtained at ages 7 and 14. The immediate soft-tissue response was assessed using stereophotogrammetric facial images acquired with and without the dentures at age 14. Findings were summarized descriptively without inferential testing.

Results

Maxillary sagittal deficiency and a skeletal Class III relationship persisted at both assessments, with the A-point–nasion–B-point angle remaining negative (−9.21° at 7 years and −5.01° at 14 years). Denture-based transverse dimensions increased, particularly in the middle and posterior regions, although anterior and posterior widths remained below age-matched reference ranges at 14 years. Tissue-bearing surface comparisons showed predominantly posterior changes in the maxilla and broader

middle-to-posterior changes in the mandible. Point A displaced 3.07 mm anteriorly and 5.34 mm inferiorly, whereas Menton displaced 6.25 mm anteriorly and 9.08 mm inferiorly; both gonial regions displaced posteriorly and inferiorly. Complete-denture insertion produced immediate soft-tissue displacement mainly in the cheeks, lips, chin, and lower facial third, with a maximum three-dimensional deviation of 6.60 mm.

Conclusions

During the 7-year observation period, persistent maxillary and midfacial sagittal deficiency, regionally heterogeneous prosthetic changes, and pronounced mandibular remodeling were observed. Multimodal assessment provided complementary information on skeletal, prosthetic and immediate soft-tissue changes. Because this was a single-patient descriptive study with only two major skeletal imaging time points, the findings cannot establish a causal treatment effect and require validation in larger longitudinal studies.

Keywords

X-linked hypohidrotic ectodermal dysplasia; congenital anodontia; craniofacial development; complete denture rehabilitation; cone-beam computed tomography; three-dimensional imaging; longitudinal study

Background

X-linked hypohidrotic ectodermal dysplasia (XLHED) is the most common inherited form of hypohidrotic ectodermal dysplasia (HED). It is caused primarily by pathogenic variants in the *EDA* gene and is characterized by hypotrichosis,

hypohidrosis or anhidrosis, and severe tooth agenesis [1]. Affected individuals may also exhibit a characteristic craniofacial phenotype, including midfacial hypoplasia, relative maxillary retrusion, and a prominent chin [2]. Evidence from experimental models suggests that impaired EDA signaling may affect craniofacial bone homeostasis. However, its relevance to craniofacial growth in humans remains uncertain [3].

Severe oligodontia or congenital anodontia create additional challenges for craniofacial development and oral rehabilitation because tooth eruption, periodontal ligament function, and normal occlusal loading are absent. Growing children may therefore require removable prostheses that are adjusted or remade periodically as their craniofacial morphology and prosthetic space change. Digital technologies, including facial scanning, cone-beam computed tomography (CBCT), and virtual design, have expanded the options for prosthodontic assessment in children with ectodermal dysplasia [4]. Cephalometry remains useful for evaluating overall sagittal and vertical relationships. Three-dimensional (3D) imaging and CBCT superimposition provide complementary information on regional skeletal displacement and remodeling [2, 5–7].

Longitudinal 3D evidence in HED remains limited. In an 8-year study of 12 children with HED, Dellavia et al. reported reduced facial growth and changes that varied by anatomical region and direction. Deficiencies in facial depth and midfacial dimensions persisted throughout the observation period [8]. However, previous longitudinal studies have focused mainly on facial dimensions. They have not concurrently evaluated regional 3D skeletal displacement, changes in prosthetic space

and denture-bearing conditions, and the immediate soft-tissue response to prosthesis insertion during staged rehabilitation.

To address this gap, we conducted a 7-year retrospective longitudinal case study of a child with genetically confirmed XLHED and congenital anodontia. The assessment integrated cephalometry, anterior cranial-base voxel-based CBCT superimposition, digital analysis of complete dentures obtained at ages 7 and 14, and 3D facial imaging at age 14. The study aimed to characterize longitudinal changes in the craniofacial skeleton, prosthetic space, and denture-bearing conditions during staged complete-denture rehabilitation. It also aimed to quantify the immediate facial soft-tissue response to denture insertion at age 14. This multimodal approach provides a patient-specific quantitative description across an important period of craniofacial growth and may help inform individualized longitudinal prosthodontic management.

Methods

Study design and participant

This retrospective longitudinal case study was based on existing clinical records and multimodal 3D data from a single child with congenital anodontia associated with XLHED. The study was designed to characterize craniofacial changes during growth and staged prosthodontic rehabilitation. The study protocol was approved by the Ethics Committee of the Hospital of Stomatology, Hebei Medical University (approval No. 2021-017). Written informed consent to participate was obtained from the patient's legal guardian.

In 2016, a male child with congenital anodontia first presented to the Department of Prosthodontics, Hospital of Stomatology, Hebei Medical University. Clinical

examination revealed characteristic features of HED, including sparse hair, hypohidrosis, and the complete absence of both primary and permanent dentitions. PCR amplification of the coding exons of the *EDA* gene followed by Sanger sequencing identified the c.1046C>T (p.Ala349Val) missense variant, which was previously reported in our earlier publication [9]. On the basis of the clinical phenotype, molecular genetic findings, and previously reported functional evidence, the patient was diagnosed with XLHED. The present study addressed a distinct research question by analyzing longitudinal craniofacial, prosthetic, and facial imaging data collected from 7 to 14 years of age that had not previously been reported or analyzed for this research purpose. These data were used to further characterize craniofacial growth in this patient with XLHED, particularly maxillary and mandibular development and regional skeletal remodeling during childhood and adolescence.

In 2017, at 7 years of age, the patient underwent the baseline CBCT examination included in this study using a NewTom VGi CBCT system (NewTom QR s.r.l., Imola, Italy). He subsequently received maxillary and mandibular complete dentures and underwent staged prosthodontic management with annual follow-up.

The dentures were adjusted or remade as needed according to their fit, the occlusal relationships, and craniofacial growth. The approximate interval between denture replacements was 1 year. The present analysis included clinical follow-up records, CBCT images acquired in 2017 and 2024, and the preserved complete dentures fabricated at ages 7 and 14. At the 2024 follow-up, additional 3D facial scans were

acquired both with and without the complete dentures in place using a 3dMDface System (3dMD LLC, Atlanta, GA, USA).

Digital scanning and 3D analysis of complete dentures

The maxillary and mandibular complete dentures preserved from the 2017 and 2024 follow-up visits were digitized by the same trained operator using a calibrated Medit T8 extraoral scanner (MEDIT Corporation, Seoul, South Korea). Before scanning, each denture was cleaned, dried, and securely positioned on the scanning platform. The occlusal and tissue-bearing surfaces and peripheral borders were captured using a standardized scanning protocol. Minor scanning defects were corrected using the scanner software. The complete datasets were then exported as standard tessellation language (STL) files and imported into Geomagic Studio 2014 (3D Systems, Inc., Rock Hill, SC, USA) for analysis.

Because the patient had congenital complete anodontia, the artificial dentitions and tissue-bearing surfaces were treated as longitudinal records of prosthetic space and denture-bearing conditions rather than as direct representations of the natural dental or skeletal arches. Denture-based arch width was measured at three anteroposterior levels. Anterior width was defined as the distance between the cusp tips of the bilateral artificial canines, whereas middle width was defined as the distance between the central fossae of the bilateral artificial second premolars. Posterior width was determined using age-specific artificial-tooth landmarks. At age 7, it was measured between the distal marginal-ridge points of the bilateral artificial second primary molars; at age 14, it was measured between the central fossae of the bilateral artificial first molars. Because

different posterior landmarks were used at the two time points, changes in posterior width were interpreted descriptively as changes in the transverse dimensions of the prostheses.

For the 3D comparison of the denture-bearing surfaces, the 2017 and 2024 maxillary models were oriented using a standardized procedure and superimposed; the same procedure was applied separately to the mandibular models. The corresponding tissue-bearing surfaces were compared using surface-deviation analysis, and color-coded deviation maps were generated to show the spatial distribution of differences between the two time points. These differences were interpreted as regional changes in denture-bearing conditions during growth rather than as direct measures of skeletal or natural dental-arch growth.

CBCT image acquisition

Craniofacial CBCT images were acquired in 2017 and 2024 using the same NewTom VGi CBCT system (NewTom QR s.r.l.). For both examinations, the dentures were removed, the patient's head was stabilized, and the scan was acquired in a standardized natural head position. Natural head position has been shown to provide a reproducible orientation for craniofacial assessment [10]. The Digital Imaging and Communications in Medicine (DICOM) datasets were imported into OnDemand3D Application 2.0 (Cybermed Inc., Daejeon, South Korea) for 3D reconstruction, anterior cranial-base registration, and subsequent analyses.

CBCT superimposition and establishment of the 3D coordinate system

The 2017 and 2024 CBCT datasets were imported into OnDemand3D, with the 2017 scan designated as the baseline reference volume and the 2024 scan as the follow-

up volume. Head orientation was initially standardized in multiplanar reconstruction (MPR) views to obtain comparable midsagittal and horizontal orientations in the two scans. The 2024 volume was then coarsely aligned with the anterior cranial-base region of the 2017 volume. Automatic grayscale voxel-based registration was subsequently performed using the software's built-in registration algorithm. Anterior cranial-base voxel-based registration has demonstrated good reliability and reproducibility for serial CBCT superimposition in growing patients [11, 12].

The reference region comprised relatively stable structures of the anterior cranial base, including the cribriform plate, planum sphenoidale, floor of the sella turcica, anterior portion of the dorsum sellae, and medial aspects of both lesser wings of the sphenoid. This extended reference region was selected because it has demonstrated greater reliability and reproducibility than more restricted midline anterior cranial-base regions [12, 13].

After registration, the quality of the superimposition was assessed visually in axial, coronal, and sagittal MPR views. The overlap of the cribriform plate, planum sphenoidale, sella turcica, and bilateral lesser wings of the sphenoid was examined. Registration was considered acceptable when no visible double contours or anatomical misalignment were present within the reference region. If discrepancies were detected, the initial alignment and voxel-based registration procedures were repeated.

After satisfactory registration, a common patient-specific 3D coordinate system was established using the 3D Ceph module of OnDemand3D. The coordinate system was defined using the 2017 reference volume and applied unchanged to the registered

2024 volume. Sella (S) was designated as the origin. The anteroposterior axis (Y-axis) was defined by the direction from S to Nasion (N), with positive values indicating anterior displacement. The transverse axis (X-axis) was perpendicular to the standardized midsagittal plane, with positive values directed toward the patient's left side. The vertical axis (Z-axis) was perpendicular to the X- and Y-axes, with positive values directed superiorly. All 3D landmark coordinates and directional displacements between 2017 and 2024 were calculated within this common coordinate system (Fig. 1).



Fig. 1 Establishment of the three-dimensional coordinate system after anterior cranial-base registration. Sella (S) was defined as the origin. The direction from Sella to Nasion (N) defined the anteroposterior axis (Y-axis), with positive values directed anteriorly. The transverse axis (X-axis) was perpendicular to the midsagittal plane, with positive values directed toward the patient's left side. The vertical axis (Z-axis) was directed superiorly.

3D facial data acquisition and analysis

At the 2024 follow-up, 3D facial images were acquired with and without the complete dentures in place. Both scans were obtained during the same session by the same experienced clinician using a calibrated 3dMDface System (3dMD LLC). Before imaging, the system was calibrated according to the manufacturer's instructions. The patient was seated upright in a natural head position, with the facial muscles relaxed,

the eyes directed forward, and the mandible maintained in the physiologic rest position. The resulting facial datasets were exported as STL files for analysis.

The STL datasets were imported into Geomagic Studio 2014 (3D Systems). Initial landmark-based alignment was performed using the bilateral endocanthia, exocanthia, tragi, and soft-tissue nasion. Local surface-based best-fit registration was then performed using relatively stable central facial regions considered minimally affected by denture insertion. These regions included the forehead, nasal root, nasal dorsum, and periorbital areas. Regions potentially affected by denture-related soft-tissue support, including the nasal alae, perioral region, lips, cheeks, and chin, were excluded from the best-fit registration to minimize the influence of local soft-tissue deformation on registration accuracy.

After registration, 3D surface-deviation analysis was performed, and a color-coded map was generated to display the spatial distribution of differences between the facial surfaces acquired with and without the dentures. Point-to-point distances between the corresponding registered surfaces were calculated to quantify the immediate soft-tissue surface displacement associated with denture insertion [14].

Landmark definition and measurement analysis

Landmark identification and measurement analysis were performed using digital lateral cephalograms and 3D CBCT reconstructions to characterize craniofacial hard- and soft-tissue changes during growth. Cephalometric analysis included landmarks of the cranial base, maxilla, mandible, and facial soft tissues. It was used primarily to

assess sagittal maxillomandibular relationships, vertical facial proportions, mandibular growth patterns, and changes in the soft-tissue profile.

The 3D CBCT analysis included selected anatomical landmarks of the anterior cranial base, maxilla, and mandible. The coordinates of each landmark were recorded within the common 3D coordinate system in the transverse (X-axis), anteroposterior (Y-axis), and vertical (Z-axis) directions. Directional displacement along each axis was calculated as the difference between the 2024 and 2017 coordinates. Total 3D displacement between the two time points was also calculated from the three directional components to characterize region-specific craniofacial growth and remodeling.

Measurement protocol and repeated measurements

All cephalometric measurements, 3D CBCT landmark identification and coordinate measurements, and digital denture-model measurements were performed by the same trained investigator. To minimize intra-examiner measurement variability, each measurement was repeated three times at 2-week intervals, with the investigator blinded to the previous values. The mean of the three measurements was used in the final descriptive analysis.

Data analysis

Because the study included only one patient, all data were analyzed descriptively. No hypothesis testing or inferential statistical analyses were performed. Digital measurements were calculated and exported using the respective software packages. The findings are reported as observed values and changes between the two assessment time points.

Results

Clinical findings

The patient's height increased from 120 cm at age 7 to 165 cm at age 14, while his body weight increased from 20.0 to 42.5 kg. These values corresponded to increases of 45 cm and 22.5 kg, respectively, over the 7-year follow-up period. The clinical characteristics recorded at both time points are summarized in Table 1.

At both assessments, the patient exhibited clinical features of XLHED, including sparse scalp hair, sparse eyebrows and eyelashes, dry skin, impaired sweating, and complete anodontia. Frontal bossing, a saddle nose, thick lips, and periorbital hyperpigmentation were more pronounced at age 14 than at age 7 (Fig. 2).

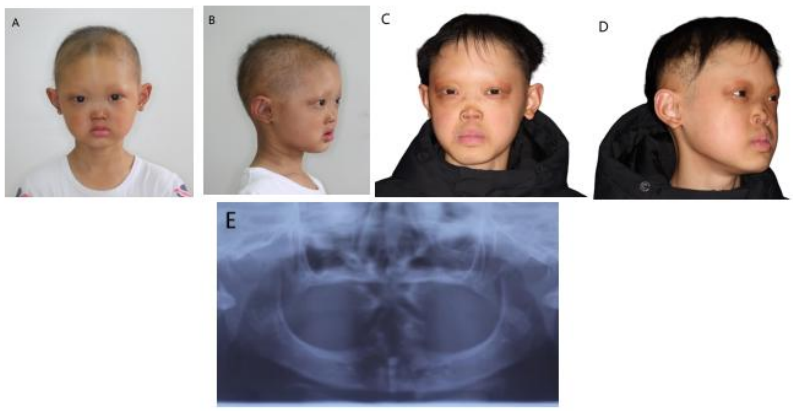


Fig. 2 Clinical facial appearance of the patient with XLHED at 7 and 14 years of age.
A, B: Frontal and lateral facial photographs at 7 years of age.
C, D: Frontal and lateral facial photographs at 14 years of age.
E: Panoramic radiograph.

Denture-based arch-width changes

Denture-based arch widths were measured in the anterior, middle, and posterior regions of the maxillary and mandibular artificial dentitions (Fig. 3). At age 7, the middle and posterior widths of both arches were below the corresponding age-matched reference ranges, with the largest discrepancies observed in the posterior regions. All measured widths had increased by age 14. The maxillary middle width was within the

reference range, whereas the mandibular middle width approached its lower limit. Despite increasing, the anterior and posterior widths of both arches remained below the corresponding reference ranges at age 14. The calculated annualized increases ranged from 0.42 to 1.08 mm/year and were greatest in the posterior region of each arch (Table 2). Because posterior width was measured using different age-specific artificial-tooth landmarks, changes in this region were interpreted descriptively as changes in posterior prosthetic transverse dimensions.

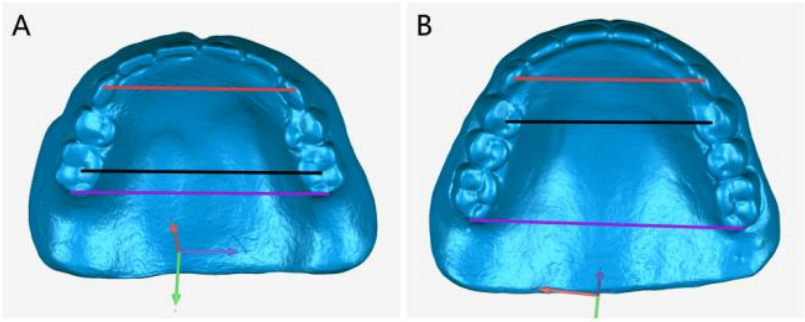


Fig. 3 Schematic illustration of denture-based arch-width measurements.

Digital denture analysis

The 3D superimposition showed that the maxillary and mandibular dentures obtained at age 14 were greater in overall length and width than those obtained at age 7 (Fig. 4). In the maxilla, differences in the tissue-bearing surface were limited anteriorly and concentrated mainly in the maxillary tuberosity and posterior hard palate. In the mandible, the differences were more extensive and involved predominantly the middle and posterior denture-bearing regions, with larger unmatched areas posteriorly. Thus, changes in the maxillary tissue-bearing surface were localized primarily to the posterior region, whereas those in the mandible were distributed more broadly across the middle and posterior regions.

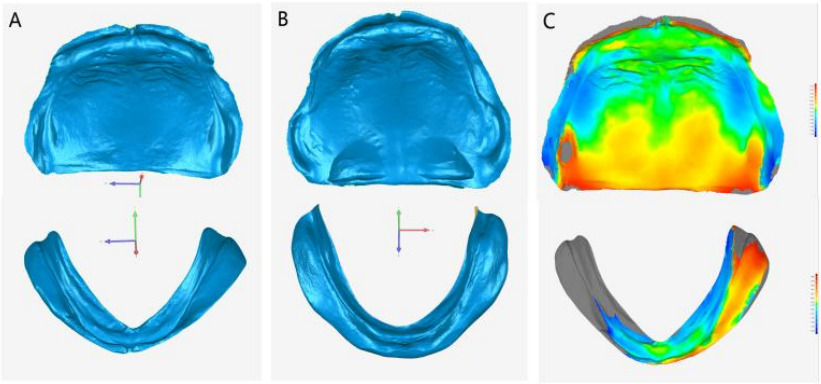


Fig. 4 Three-dimensional superimposition and color-coded deviation maps of the complete-denture tissue-bearing surfaces at 7 and 14 years of age. A: Maxillary and mandibular models at 7 years; B: corresponding models at 14 years; C: maxillary and mandibular deviation maps, respectively. Green indicates minimal deviation, red positive deviation, blue negative deviation, and gray unmatched regions.

Cephalometric analysis

The cephalometric measurements are summarized in Table 3. SNA increased from 72.77° at age 7 to 74.64° at age 14, although it remained below the reference range at both assessments. SNB decreased from 81.98° to 79.66° and remained close to the reference value. ANB became less negative, increasing from −9.21° to −5.01°, but continued to indicate a skeletal Class III relationship at age 14.

The vertical measurements also increased. MP–SN increased from 23.41° to 26.58°, while FH–MP increased from 12.36° to 16.06°; both remained below their respective reference ranges at both time points. Selected soft-tissue angular measurements, including the Z angle, FH–N′Pog′, and N′–Sn–Pog′, also remained outside their corresponding reference ranges at both assessments. Superimposition of the lateral cephalometric tracings on the anterior cranial base (S–N) showed close overlap in the cranial-base region. The principal contour changes occurred in the maxillary, mandibular, and lower facial regions (Fig. 5).

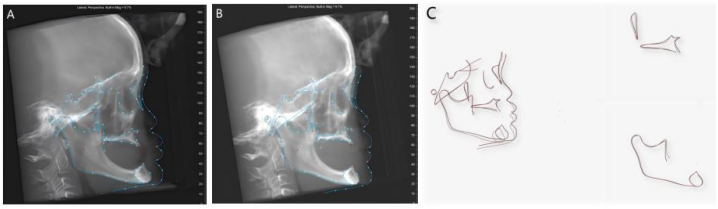


Fig. 5 Cephalometric evaluation of the patient with XLHED at 7 and 14 years of age. A: Lateral cephalogram at 7 years. B: Lateral cephalogram at 14 years. C: Superimposition of the lateral cephalometric tracings at 7 and 14 years. The registration reference used for superimposition is described in the Methods.

Craniofacial skeletal changes

Voxel-based registration of the 2017 and 2024 CBCT datasets produced close overlap of the anterior cranial-base reference structures, indicating satisfactory registration (Fig. 6A and B).

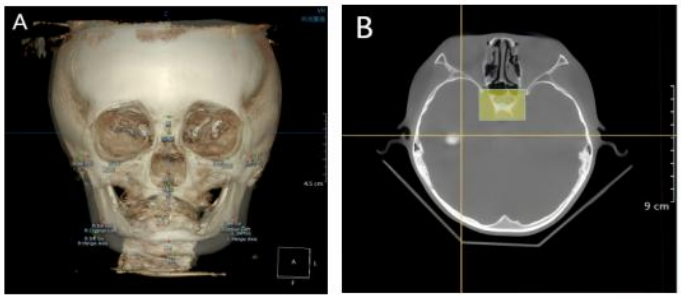


Fig. 6 Three-dimensional CBCT superimposition between 7 and 14 years of age following anterior cranial-base registration.
A: Frontal view of the superimposed three-dimensional CBCT models. B: Axial view illustrating the anterior cranial-base reference region used for voxel-based registration

The 3D CBCT measurements are summarized in Table 4. Between ages 7 and 14, the anterior maxillary landmarks displaced predominantly in the anterior and inferior directions. No transverse displacement was recorded for either ANS or point A. ANS displaced 2.38 mm anteriorly and 6.30 mm inferiorly, while point A displaced 3.07 mm anteriorly and 5.34 mm inferiorly. Nasion displaced primarily in the anterior direction (4.83 mm), with only 0.37 mm of inferior displacement.

The mandibular changes were more pronounced and varied among anatomical regions. Menton displaced 6.25 mm anteriorly and 9.08 mm inferiorly. By contrast, the

right and left inferior gonial landmarks displaced posteriorly by 2.05 and 2.79 mm and inferiorly by 8.74 and 6.87 mm, respectively. Both Porion landmarks also displaced posteriorly. Their vertical displacements were relatively small and occurred in different directions on the two sides.

Overall, the maxilla showed relatively limited anterior displacement, whereas the mandible exhibited more pronounced vertical and region-specific changes. These changes were characterized by anterior-inferior displacement of Menton and posterior-inferior displacement of the bilateral gonial regions (Fig. 6; Table 4).

3D facial soft-tissue changes

At age 14, comparison of the 3D facial scans acquired with and without the complete dentures showed that the immediate soft-tissue differences were concentrated mainly in the bilateral cheeks, lips, and chin. The greatest deviations occurred in the lower facial third (Fig. 7). In contrast, relatively small differences were observed in the forehead, periorbital, and zygomatic regions. The maximum 3D surface deviation between the two conditions was 6.60 mm.

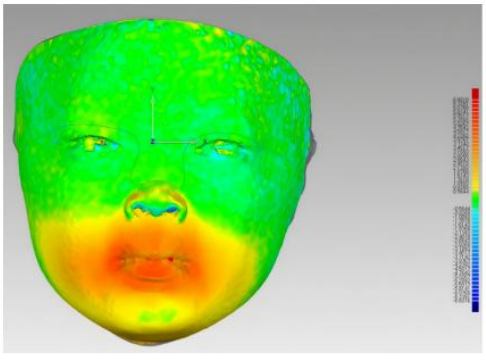


Fig. 7 Three-dimensional facial soft-tissue deviation analysis with and without the complete dentures in place at 14 years of age. The color-coded deviation map shows point-to-point surface differences between the two facial scans. Green indicates minimal surface deviation, red positive deviation, and blue negative deviation.

Discussion

This study combined longitudinal analysis of digital complete-denture models and anterior cranial-base CBCT superimposition with a within-session 3D facial comparison to characterize craniofacial and prosthetic changes in a child with genetically confirmed XLHED and congenital anodontia from ages 7 to 14. The findings showed persistent sagittal deficiency of the maxilla and midface, regionally heterogeneous changes in prosthetic space and denture-bearing conditions, and pronounced vertical and region-specific mandibular remodeling. The mandibular changes were characterized by anterior-inferior displacement of Menton and posterior-inferior displacement of the bilateral gonial regions. At age 14, denture insertion was associated with immediate soft-tissue surface displacement, particularly in the perioral region and lower facial third. These findings should be interpreted cautiously because they are based on a single patient and only two major skeletal imaging time points. Consequently, a continuous growth trajectory could not be established, and the relative contributions of natural growth, the XLHED phenotype, congenital anodontia, and prosthodontic management could not be distinguished.

Regional changes in prosthetic space and denture-bearing conditions

A distinctive feature of this study was the availability of complete dentures fabricated at different stages of growth, which served as patient-specific longitudinal records of prosthetic space and denture-bearing conditions. Digital comparison of the dentures obtained at ages 7 and 14 showed greater transverse changes in the middle and posterior regions of the artificial dentitions than in the anterior regions. The 3D comparison of the tissue-bearing surfaces revealed a similar pattern. The most

pronounced maxillary differences occurred in the tuberosity and posterior hard palate, whereas the mandibular differences extended across the middle and posterior denture-bearing regions. In both arches, changes in the anterior region were comparatively limited.

These measurements should not be interpreted as indicators of natural dental-arch or skeletal-arch growth. The dimensions of the artificial dentitions and denture bases were influenced by several factors, including residual ridge morphology, maxillomandibular relationships, occlusal requirements, denture stability, border extension, and artificial-tooth arrangement at each treatment stage. Although some denture-based widths approached age-matched reference ranges derived from natural dentitions at age 14, this finding indicates a stage-specific increase in prosthetic space rather than normalization of the underlying skeletal arch. Similarly, the observed differences between the tissue-bearing surfaces may reflect the combined effects of craniofacial growth, local skeletal remodeling, functional loading, and changes in prosthetic design. The individual contribution of each factor cannot be determined from the available data.

Overall, the regional differences in the artificial dentitions and tissue-bearing surfaces suggest that prosthodontic requirements changed unevenly across the denture-bearing regions during growth. The longitudinal digital denture records should therefore be regarded as clinically relevant measures of stage-specific changes in prosthetic space and denture-base adaptation rather than as surrogates for natural dental-arch growth. These records complement the skeletal information obtained from

CBCT and support individualized reassessment and periodic modification of removable prostheses throughout craniofacial growth [17, 18].

Maxillomandibular growth and regional remodeling during prosthodontic rehabilitation

A key feature of this study was the combined use of longitudinal cephalometry and anterior cranial-base CBCT superimposition. Cephalometry characterized the overall sagittal and vertical jaw relationships, whereas CBCT superimposition localized the direction and magnitude of regional skeletal displacement. Over the 7-year observation period, the anterior maxilla showed relatively limited anterior displacement accompanied by an inferior component. In contrast, the mandible exhibited a regionally differentiated pattern, with anterior-inferior displacement of Menton and posterior-inferior displacement of the bilateral gonial regions. Together with the increases in MP–SN and FH–MP, these findings suggest that the change in the overall maxillomandibular relationship reflected different patterns of displacement across skeletal regions rather than uniform forward growth of the maxilla and mandible.

The persistent maxillary and midfacial sagittal deficiency observed in this patient is consistent with previous reports of HED and XLHED. Using 3D craniofacial morphometry, Goodwin et al. demonstrated midfacial deficiency accompanied by relative mandibular prominence [2]. Lexner et al. similarly reported reduced maxillary length and prognathism, with relatively preserved mandibular dimensions, in individuals with XLHED [19]. Longitudinal 3D studies have also demonstrated region- and direction-specific facial growth in HED. Facial width and height increased during adolescence, whereas the deficiency in midfacial depth persisted [8]. Differences in the

magnitude and timing of growth relative to reference subjects have also been reported [20]. These observations are consistent with the persistently reduced SNA and relatively limited anterior displacement of ANS and point A in the present patient.

The combined two-dimensional (2D) and 3D assessments provided complementary information on how regional skeletal changes contributed to the overall cephalometric pattern. In particular, the divergent displacement of Menton and the gonial regions could not be fully characterized using angular cephalometric measurements alone. This pattern is consistent with 3D evidence that mandibular growth involves region-specific changes in shape and proportion rather than simple proportional enlargement [6]. However, the sagittal trajectory observed in the present patient differed from that reported by Bondarets et al., who found a tendency toward an increasingly pronounced Class III relationship in individuals with syndromic ectodermal dysplasia [21]. In the present patient, ANB became less negative, increasing from −9.21° to −5.01°, although the skeletal Class III relationship persisted. This difference may reflect variation in phenotype, the severity of tooth agenesis, individual growth patterns, and treatment background.

Importantly, these skeletal changes occurred during continuous prosthodontic rehabilitation but cannot be attributed to the prostheses themselves. Nomura et al. similarly reported continued maxillomandibular growth in a patient with HED and complete anodontia who underwent long-term complete-denture treatment [22]. Because the patient lacked an untreated control period and skeletal imaging was limited to two time points, the observed changes must be interpreted as region-specific

maxillomandibular growth and remodeling during staged prosthodontic rehabilitation. These adaptations likely reflect the combined influences of intrinsic growth, the XLHED phenotype, congenital anodontia, and functional prosthodontic adaptation.

Immediate facial soft-tissue response to denture insertion

The 3D facial imaging at age 14 demonstrated that complete-denture insertion elicited immediate soft-tissue displacement predominantly within the perioral and lower facial regions. The most pronounced outward displacement occurred at the upper and lower lips, oral commissures, cheeks, mentolabial sulcus, and chin, whereas the forehead, nasal root, and periorbital regions exhibited minimal change. This regional distribution reflects the mechanical support restored to the lips and cheeks by the artificial dentition and denture bases, alongside the re-establishment of the occlusal vertical dimension. Consequently, complete dentures provided immediate soft-tissue support and enhanced lower facial contour during wear in this patient with XLHED and congenital anodontia.

These findings are consistent with previous prosthodontic reports involving children with ectodermal dysplasia. Tarjan et al. reported that removable prostheses improved facial esthetics, speech, and masticatory function in young patients with HED [23]. The American College of Prosthodontists similarly recognizes removable partial or complete dentures as an early and minimally invasive treatment option for improving appearance and function in growing patients with ectodermal dysplasia [18]. The present study adds quantitative evidence of the immediate facial response to denture

insertion through 3D surface-deviation analysis rather than relying solely on visual or conventional clinical assessment.

The regional distribution of the soft-tissue differences also agrees with findings from a 3D study of edentulous adults. In that study, comparison of facial scans obtained with and without complete dentures showed that the greatest soft-tissue changes occurred in the perioral region [14]. Although adults with edentulism differ substantially from the present pediatric patient with XLHED, the similar distribution of surface changes supports the interpretation that the observed perioral and lower facial displacement primarily reflected the mechanical support provided by the prostheses. Importantly, the present analysis represents an immediate within-session comparison of the denture-on and denture-off conditions. It should not be interpreted as evidence of long-term soft-tissue growth, permanent remodeling, or a biological treatment effect.

Clinical implications for prosthodontic management and implant timing

The integrated prosthetic and skeletal data underscore the importance of distinguishing localized adaptations in denture-bearing tissues from true underlying skeletal remodeling during childhood development. Although the anterior mandibular denture-bearing surface exhibited minimal morphological change between ages 7 and 14, voxel-based CBCT superimposition revealed ongoing regional displacement, characterized by pronounced anterior-inferior translation of Menton. Consequently, localized stability in the anterior denture-bearing area must not be misconstrued as skeletal maturity; furthermore, conventional 2D sagittal measurements alone may fail to capture complex, 3D skeletal dynamics.

This distinction is particularly relevant when considering the timing of implant placement. Osseointegrated implants remain relatively fixed while the surrounding craniofacial skeleton continues to grow and remodel. Implant placement before completion of growth may therefore lead to progressive positional and occlusal discrepancies [24]. In the present patient, the limited change observed in the anterior mandibular denture-bearing region should not, in isolation, be used to determine readiness for implant treatment. During active growth, removable prostheses allow periodic adjustment, relining, or replacement as craniofacial anatomy and denture-bearing conditions change [17, 18]. Any future implant-assisted rehabilitation should be individualized on the basis of residual craniofacial growth, local anatomical conditions, and the patient's clinical needs [18, 25, 26].

Strengths and limitations

A major strength of this study was the longitudinal evaluation of a child with genetically confirmed XLHED and congenital anodontia during an important period of craniofacial growth from ages 7 to 14. The integration of cephalometry, anterior cranial-base voxel-based CBCT superimposition, serial digital complete-denture models, and 3D facial imaging enabled complementary assessment of overall maxillomandibular relationships, regional skeletal displacement, stage-specific prosthetic changes, and the immediate soft-tissue response to denture insertion. This multimodal approach provided information that could not have been obtained using any single method and reduced the influence of interindividual variability inherent in cross-sectional comparisons.

Several limitations should be considered. First, this was a longitudinal observation of a single patient; therefore, the findings cannot be generalized to the broader XLHED population. Second, skeletal imaging was available at only two major time points. Consequently, the temporal sequence and rate of the craniofacial changes could not be determined, and a continuous growth trajectory could not be established. Third, 3D facial imaging was performed only at age 14 and captured an immediate within-session comparison of the denture-on and denture-off conditions rather than longitudinal facial soft-tissue growth. Fourth, the complete dentures were clinically adapted prosthetic records rather than direct representations of the natural dental or skeletal arches. Furthermore, no contemporaneous healthy control was available. Finally, the craniofacial changes occurred during continuous prosthodontic management and probably reflected the combined influences of natural growth, the XLHED phenotype, congenital anodontia, and functional adaptation. A causal effect of prosthodontic treatment on craniofacial growth therefore cannot be inferred.

Future studies should include larger cohorts with genetic confirmation, multiple longitudinal skeletal assessments when clinically justified, repeated radiation-free facial imaging, and standardized digital prosthetic or intraoral records. The inclusion of functional and patient-reported outcomes would further clarify craniofacial growth patterns and help optimize the timing of definitive rehabilitation.

Conclusions

In this child with XLHED and congenital anodontia, the 7-year observation period documented persistent maxillary and midfacial sagittal deficiency, region-specific

mandibular remodeling, and heterogeneous changes in prosthetic space and denture-bearing conditions during staged rehabilitation. The integration of cephalometry, 3D CBCT superimposition, digital denture analysis, and facial imaging provided complementary information on overall maxillomandibular relationships, regional skeletal displacement, stage-specific prosthetic changes, and the immediate soft-tissue response to denture insertion. These findings illustrate the potential value of individualized longitudinal assessment when modifying removable prostheses and the importance of considering residual skeletal growth before future implant rehabilitation. However, because this was a descriptive single-patient study with only two major skeletal imaging time points, no causal effect of prosthodontic treatment on craniofacial growth can be inferred. The findings should be examined further in larger longitudinal cohorts.

List of abbreviations

3D: Three-dimensional

ANB: A-point-nasion-B-point angle

ANS: Anterior nasal spine

CBCT: Cone-beam computed tomography

EDA: Ectodysplasin-A

EP: Esthetic plane

FH-MP: Frankfort horizontal-mandibular plane angle

Go: Gonion

HED: Hypohidrotic ectodermal dysplasia

Inf Go: Inferior gonion

LL-EP: Lower lip-esthetic plane distance

Me: Menton

MP-SN: Mandibular plane-sella-nasion angle

MPR: Multiplanar reconstruction

N: Nasion

Or: Orbitale

Po / Por: Porion

S: Sella

SNA: Sella-nasion-A-point angle

SNB: Sella-nasion-B-point angle

STL: Standard tessellation language

UL-EP: Upper lip-esthetic plane distance

XLHED: X-linked hypohidrotic ectodermal dysplasia

Z-angle: Z-angle

Declarations

Ethics approval and consent to participate

This retrospective study used data collected during the patient's previous clinical follow-up. The study protocol was approved by the Ethics Committee of the Hospital of Stomatology, Hebei Medical University (approval No. 2021-017). Written informed consent to participate was obtained from the patient's legal guardian.

Consent for publication

Written informed consent was obtained from the patient's parent/legal guardian for publication of the patient's non-anonymized high-resolution clinical facial photographs and other clinical data included within this manuscript.

Availability of data and materials

The datasets generated and/or analyzed during the current study are not publicly available because they contain potentially identifiable clinical and imaging data from a single pediatric patient. Data that can be sufficiently de-identified without compromising patient confidentiality are available from the corresponding author upon reasonable request and subject to applicable ethical and institutional requirements.

Competing interests

The authors declare that they have no competing interests.

Funding

This work received partial financial support from the Special Project of Health Innovation of the Hebei Provincial Department of Science and Technology of China (grant no. 21377716D) and the Natural Science Foundation of Hebei Province of China (grant no. H2022206246).

Authors' contributions

JG contributed to data curation, formal analysis, methodology, preparation of the original draft, and review and editing of the manuscript. ZS contributed to formal analysis, methodology, and preparation of the original draft. XM contributed to methodology and review and editing of the manuscript. ZY and XQ supervised the study and critically revised the manuscript. DH contributed to supervision and validation. YY and YZ contributed to data curation. JR provided guidance on the study,

contributed to the interpretation of the 2D and 3D analytical findings, and participated in manuscript preparation. WS contributed to data curation, resources, supervision, and review and editing of the manuscript. All authors read and approved the final manuscript.

Acknowledgements

The authors sincerely thank the patient and his legal guardian for their cooperation throughout the long-term clinical follow-up. The authors also gratefully acknowledge the technical support provided by the Department of Prosthodontics, Dental Laboratory, and Department of Radiology at the Hospital of Stomatology, Hebei Medical University.

Generative AI statement

ChatGPT (OpenAI) was used to assist with English-language editing and structural refinement during manuscript preparation. All AI-assisted text was critically reviewed and revised by the authors, who take full responsibility for the accuracy, integrity, and final content of the manuscript.

References

[1] Wohlfart S, Meiller R, Hammersen J, Park J, Menzel-Severing J, Melichar VO, et al. Natural history of X-linked hypohidrotic ectodermal dysplasia: a 5-year follow-up study. *Orphanet J Rare Dis*. 2020;15:7. doi:10.1186/s13023-019-1288-x.

[2] Goodwin AF, Larson JR, Jones KB, Liberton DK, Landan M, Wang Z, et al. Craniofacial morphometric analysis of individuals with X-linked hypohidrotic ectodermal dysplasia. *Mol Genet Genomic Med*. 2014;2(5):422–429. doi:10.1002/mgg3.84.

[3] Schweikl C, Maier-Wohlfart S, Schneider H, Park J. Ectodysplasin A1 deficiency

leads to osteopetrosis-like changes in bones of the skull associated with diminished osteoclastic activity. *Int J Mol Sci*. 2022;23(20):12189. doi:10.3390/ijms232012189.

[4] Yang C, Chen W, Gao J, Huang S. Application of digital virtual simulated design in the prosthodontic rehabilitation of a child with a novel EDA mutation in ectodermal dysplasia: a clinical report. *J Prosthet Dent*. 2025;134(5):1384–1390. doi:10.1016/j.prosdent.2024.07.026.

[5] Akleyin E, Yavuz Y, Yardımeden A. Three-dimensional modeling and quantitative assessment of mandibular volume in ectodermal dysplasia: a case series. *Medicina (Kaunas)*. 2024;60(4):528. doi:10.3390/medicina60040528.

[6] Klop C, Schreurs R, De Jong GA, Klinkenberg ETM, Vespasiano V, Rood NL, et al. An open-source, three-dimensional growth model of the mandible. *Comput Biol Med*. 2024;175:108455. doi:10.1016/j.compbiomed.2024.108455.

[7] Shihabi R, Liu Y, Kusaibati AM, Maraabeh F, Zhan J, Zhang J, et al. Three-dimensional analysis of mandibular and condylar growth using artificial intelligence tools: a comparison of twin-block and Frankel II appliances. *BMC Oral Health*. 2025;25:254. doi:10.1186/s12903-025-05624-z.

[8] Dellavia C, Catti F, Sforza C, Tommasi DG, Ferrario VF. Craniofacial growth in ectodermal dysplasia: an 8-year longitudinal evaluation of Italian subjects. *Angle Orthod*. 2010;80(4):733–739. doi:10.2319/101909-584.1.

[9] Wang X, Zhang Z, Yuan S, Ren J, Qu H, Zhang G, Chen W, Zheng S, Meng L, Bai J, Du Q, Yang D, Shen W. A novel EDA1 missense mutation in X-linked hypohidrotic ectodermal dysplasia. *Medicine (Baltimore)*. 2020;99(11):e19244. doi:10.1097/MD.0000000000019244.

[10] Tian K, Li Q, Wang X, Liu X, Wang X, Li Z. Reproducibility of natural head position in normal Chinese people. *Am J Orthod Dentofacial Orthop*. 2015;148(3):503–510. doi:10.1016/j.ajodo.2015.05.017.

[11] Weissheimer A, Menezes LM, Koerich L, Pham J, Cevidanes LH. Fast three-dimensional superimposition of cone beam computed tomography for orthopaedics and orthognathic surgery evaluation. *Int J Oral Maxillofac Surg*. 2015;44(9):1188–1196. doi:10.1016/j.ijom.2015.04.001.

[12] Häner ST, Kanavakis G, Matthey F, Gkantidis N. Voxel-based superimposition of serial craniofacial CBCTs: Reliability, reproducibility and segmentation effect on hard-tissue outcomes. *Orthod Craniofac Res*. 2020;23(1):92–101. doi:10.1111/ocr.12347.

[13] Ghamri M, Kanavakis G, Gkantidis N. Reliability of Different Anterior Cranial Base Reference Areas for Voxel-Based Superimposition. *J Clin Med*. 2021;10(22):5429. doi:10.3390/jcm10225429.

[14] Hernández EL, Alvarez A, Abou-Ayash S, Att W. Effect of Complete Dentures on Facial Soft Tissue Volume: A 3D Comparative Study. *Int J Prosthodont*. 2022;35(2):208–218. doi:10.11607/ijp.7057.

[15] Tian K. Normative arch-width values for Chinese children. *Chinese Journal of Orthodontics*. 2015;22(2):89–93.

[16] Zhao ZH, Bai D. Orthodontic clinical practice guidelines. Beijing: People's Medical Publishing House; 2018.

[17] Tomar S, Srivastava N, Rana V, et al. Techniques and outcomes in prosthetic rehabilitation for patients with ectodermal dysplasia: a systematic review. *Eur Arch*

Paediatr Dent. 2026;27(1):41–54. doi:10.1007/s40368-025-01125-3.

[18] American College of Prosthodontists. Dental management of persons with ectodermal dysplasia: position statement. Revised and approved August 29, 2023.

[19] Lexner MO, Bardow A, Bjorn-Jorgensen J, Hertz JM, Almer L, Kreiborg S. Anthropometric and cephalometric measurements in X-linked hypohidrotic ectodermal dysplasia. *Orthod Craniofac Res*. 2007;10(4):203–215. doi:10.1111/j.1601-6343.2007.00402.x.

[20] Dellavia C, Catti F, Sforza C, Grandi G, Ferrario VF. Non-invasive longitudinal assessment of facial growth in children and adolescents with hypohidrotic ectodermal dysplasia. *Eur J Oral Sci*. 2008;116(4):305–311. doi:10.1111/j.1600-0722.2008.00550.x.

[21] Bondarets N, Jones RM, McDonald F. Analysis of facial growth in subjects with syndromic ectodermal dysplasia: a longitudinal analysis. *Orthod Craniofac Res*. 2002;5(2):71–84. doi:10.1034/j.1600-0544.2002.01159.x.

[22] Nomura S, Hasegawa S, Noda T, Ishioka K. Longitudinal study of jaw growth and prosthetic management in a patient with ectodermal dysplasia and anodontia. *Int J Paediatr Dent*. 1993;3(1):29–38. doi:10.1111/j.1365-263x.1993.tb00044.x.

[23] Tarjan I, Gabris K, Rozsa N. Early prosthetic treatment of patients with ectodermal dysplasia: a clinical report. *J Prosthet Dent*. 2005;93(5):419–424. doi:10.1016/j.prosdent.2005.01.012.

[24] Thilander B, Odman J, Lekholm U. Orthodontic aspects of the use of oral implants in adolescents: a 10-year follow-up study. *Eur J Orthod*. 2001;23(6):715–731. doi:10.1093/ejo/23.6.715.

[25] Zhu S, Chen R, Zhang S, Wang Z, Xie Z. Outcomes of dental implant treatment in 3-18 year old children with ectodermal dysplasia: a systematic review spanning three decades. *BMC Oral Health*. 2025;25(1):1818. doi:10.1186/s12903-025-07230-5.

[26] Montanari M, Grande F, Lepidi L, Piana G, Catapano S. Rehabilitation with implant-supported overdentures in preteens patients with ectodermal dysplasia: a cohort study. *Clin Implant Dent Relat Res*. 2023;25(6):1187–1196. doi:10.1111/cid.13258.

Figure legends

Fig. 1 Establishment of the three-dimensional coordinate system after anterior cranial-base registration. Frontal and lateral views show the patient-specific coordinate system. Sella (S) was designated as the origin. The direction from S to Nasion (N) defined the anteroposterior axis (Y-axis), with positive values directed anteriorly; the transverse axis (X-axis) was perpendicular to the midsagittal plane, with positive values directed toward the patient's left side; and the vertical axis (Z-axis) was perpendicular to the X- and Y-axes, with positive values directed superiorly.

Fig. 2 Clinical facial appearance of the patient with X-linked hypohidrotic ectodermal dysplasia (XLHED) at ages 7 and 14 and panoramic radiographic evidence of complete anodontia. **(A, B)** Frontal and lateral facial photographs, respectively, at age 7. **(C, D)** Frontal and lateral facial photographs, respectively, at age 14. **(E)** Panoramic radiograph demonstrating complete anodontia.

Fig. 3 Schematic illustration of denture-based arch-width measurements on the maxillary complete dentures at ages 7 **(A)** and 14 **(B)**. The red, black, and purple lines indicate the anterior, middle, and posterior widths, respectively. Anterior width was measured between the bilateral artificial canine cusp tips, and middle width between the bilateral artificial second-premolar central fossae. Posterior width was measured

between the distal marginal-ridge points of the bilateral artificial second primary molars at age 7 and between the central fossae of the bilateral artificial first molars at age 14.

Fig. 4 Three-dimensional superimposition and color-coded deviation maps of the tissue-bearing surfaces of the complete dentures at ages 7 and 14. **(A)** Maxillary and mandibular denture models at age 7. **(B)** Corresponding models at age 14. **(C)** Color-coded surface-deviation maps of the maxillary and mandibular dentures, respectively. Green indicates minimal deviation, red positive deviation, blue negative deviation, and gray unmatched regions.

Fig. 5 Cephalometric evaluation of the patient with XLHED at ages 7 and 14. **(A)** Lateral cephalogram at age 7. **(B)** Lateral cephalogram at age 14. **(C)** Superimposition of the lateral cephalometric tracings at ages 7 and 14 using the anterior cranial base (S–N) as the registration reference.

Fig. 6 Three-dimensional CBCT superimposition of the scans acquired at ages 7 and 14 following anterior cranial-base registration. **(A)** Frontal view of the superimposed three-dimensional CBCT models. **(B)** Axial view showing the anterior cranial-base reference region used for voxel-based registration.

Fig. 7 Three-dimensional facial soft-tissue deviation analysis comparing scans acquired with and without the complete dentures at age 14. The color-coded deviation map shows the point-to-point surface differences between the two facial scans. Green indicates minimal surface deviation, red positive deviation, and blue negative deviation.

767

768 **Table**

769 Table 1. Clinical characteristics of the patient with XLHED at ages 7 and 14

Characteristic	Age 7	Age 14	Change over 7 years
Height (cm)	120	165	Increased by 45 cm
Body weight (kg)	20.0	42.5	Increased by 22.5 kg
Hair	Sparse, fine, yellowish scalp hair; sparse eyebrows and eyelashes	Sparse scalp hair with larger areas of alopecia in the temporal and periauricular regions; sparse eyebrows and eyelashes	Slight progression of hair sparsity
Dentition	Complete absence of primary and permanent teeth	Complete absence of primary and permanent teeth	No change
Skin	Dry skin with periorbital wrinkling	Less pronounced skin dryness; persistent periorbital wrinkling	Skin dryness became less evident; periorbital wrinkling persisted
Sweating	Anhidrosis with heat intolerance in summer	Hypohidrosis with a tendency to overheat after exercise	Reported improvement in sweating ability
Facial features	Mild frontal bossing and saddle nose	More pronounced frontal bossing and saddle nose, with periorbital hyperpigmentation and thick lips	Facial features of XLHED became more pronounced

770 Note: XLHED, X-linked hypohidrotic ectodermal dysplasia.

771

772 Table 2. Denture-based arch-width measurements at ages 7 and 14 and comparisons with age-matched reference ranges

Measurement	Age 7 measurement	Age 7 reference range	Difference from lower limit at age 7	Age 14 measurement	Age 14 reference range	Difference from lower limit at age 14	Annualized increase (mm/year)
Maxillary anterior width	26.75	28–32	−1.25	31.60	33–37	−1.40	0.69
Maxillary middle width	32.86	40–44	−7.14	38.52	38–42	0.52	0.81
Maxillary posterior width	35.41	45–48	−9.59	42.94	49–53	−6.06	1.08
Mandibular anterior width	20.40	22–26	−1.60	23.42	25–29	−1.58	0.43
Mandibular middle width	28.97	32–36	−3.03	31.93	32–36	−0.07	0.42
Mandibular posterior width	31.62	38–42	−6.38	39.19	43–47	−3.81	1.08

Notes: Measurements, reference ranges, and differences from the lower limit are expressed in millimeters. Age-matched reference ranges were obtained from Ref. [15]. Difference from lower limit was calculated as the measured width minus the lower limit of the corresponding reference range; negative values indicate measurements below the lower limit. Annualized increase was calculated as the difference between the measurements at ages 14 and 7 divided by 7 years. Posterior width was measured using age-specific artificial-tooth landmarks: the distal marginal-ridge points of the bilateral artificial second primary molars at age 7 and the central fossae of the bilateral artificial first molars at age 14. These comparisons are descriptive because the denture-based measurements represent prosthetic dimensions rather than natural dental-arch or skeletal-arch widths.

Table 3. Cephalometric measurements at ages 7 and 14 compared with reference values

Measurement	Reference value, mean ± SD	Age 7	Age 14
SNA (°)	84.0 ± 3.0	72.77	74.64
SNB (°)	80.0 ± 3.0	81.98	79.66
ANB (°)	4.0 ± 2.0	−9.21	−5.01
MP–SN (°)	35.0 ± 4.0	23.41	26.58
FH–MP (°)	29.0 ± 4.0	12.36	16.06
UL–EP (mm)	2.0 ± 2.0	1.01	2.06
LL–EP (mm)	3.0 ± 3.0	2.34	0.08
Z angle (°)	69.0 ± 5.0	88.96	88.34
FH–N′Pog′ (°)	80.0 ± 3.0	102.43	98.68
N′–Sn–Pog′ (°)	165.0 ± 4.0	186.56	181.90

Note: Reference values are presented as reported in Ref. [16] and were used only for descriptive comparison. SNA, sella–nasion–point A angle; SNB, sella–nasion–point B angle; ANB, point A–nasion–point B angle; MP–SN, angle between the mandibular plane and the sella–nasion line; FH–MP, angle between the Frankfort horizontal plane and the mandibular plane; UL–EP, upper-lip-to-esthetic-plane distance; LL–EP, lower-lip-to-esthetic-plane distance; Z angle, angle between the Frankfort horizontal plane and the profile line connecting the most protrusive lip with soft-tissue pogonion; FH–N′Pog′, angle between the Frankfort horizontal plane and the soft-tissue facial plane; N′–Sn–Pog′, soft-tissue facial convexity angle; N′, soft-tissue nasion; Sn, subnasale; Pog′, soft-tissue pogonion; SD, standard deviation.

Table 4. Three-dimensional coordinates and directional displacements of selected craniofacial landmarks between ages 7 and 14 after anterior cranial-base registration

Landmark	Coordinates at age 7, X/Y/Z (mm)	Coordinates at age 14, X/Y/Z (mm)	ΔX (mm)	ΔY (mm)	ΔZ (mm)
N	−0.02 / 55.48 / 10.55	0.38 / 60.31 / 10.18	0.40	4.83	−0.37
S	0.00 / 0.00 / 0.00	0.00 / 0.00 / 0.00	0.00	0.00	0.00
R Po	−49.63 / −19.04 / −15.66	−54.67 / −21.85 / −16.77	−5.04	−2.81	−1.11
L Po	50.18 / −20.92 / −15.92	53.61 / −23.49 / −15.17	3.43	−2.57	0.75
R Or	−32.54 / 46.79 / −15.66	−36.07 / 48.01 / −17.83	−3.53	1.22	−2.17
L Or	30.62 / 46.79 / −15.66	36.21 / 48.01 / −17.83	5.59	1.22	−2.17
ANS	0.00 / 50.91 / −27.12	0.00 / 53.29 / −33.42	0.00	2.38	−6.30
A	0.00 / 48.87 / −31.87	0.00 / 51.94 / −37.21	0.00	3.07	−5.34
Me	0.00 / 52.82 / −71.90	2.18 / 59.07 / −80.98	2.18	6.25	−9.08
R Inf Go	−40.03 / 1.27 / −57.46	−44.70 / −0.78 / −66.20	−4.67	−2.05	−8.74
L Inf Go	39.38 / −0.41 / −55.84	45.32 / −3.20 / −62.71	5.94	−2.79	−6.87

Note: Coordinates and directional displacements are reported in millimeters according to the three-dimensional coordinate system defined in the Methods. Directional displacement was calculated as the coordinate at age 14 minus the corresponding coordinate at age 7. Positive X-values indicate displacement toward the patient's left side, positive Y-values indicate anterior displacement, and positive Z-values indicate superior displacement; negative values values indicate displacement toward the right, posteriorly, and inferiorly, respectively. N, nasion; S, sella; Po, porion; Or, orbitale; ANS, anterior nasal spine; A, point A; Me, menton; Inf Go, inferior gonion; R, right; L, left.